Acta Oceanol. Sin., 2013, Vol. 32, No. 11, P. 10-20
DOI: 10.1007/s13131-013-0372-7
http://www.hyxb.org.cn
E-mail: hyxbe@263.net

Rainfall effect on wind waves and the turbulence beneath air-sea interface

ZHAO Dongliang[1*], MA Xin[1], LIU Bin[2], XIE Lian[2]

[1] Physical Oceanography Laboratory, Ocean University of China, Qingdao 266100, China
[2] Department of Marine, Earth and Atmospheric Sciences, North Carolina State University, Raleigh 27695–8208, USA

Received 13 February 2012; accepted 7 April 2013

Abstract
Rainfall effects on wind waves and turbulence are investigated through the laboratory experiments in a large wind-wave tank. It is found that the wind waves are damped as a whole at low wind speeds, but are enhanced at high wind speeds. This dual effect of rain on the wind waves increases with the increase of rain rate, while the influence of rainfall-area length is not observable. At the low wind speed, the corresponding turbulence in terms of the turbulent kinetic energy (TKE) dissipation rate is significantly enhanced by rainfall as the waves are damped severely. At the high wind speed, the augment of the TKE dissipation rate is suppressed while the wind waves are enhanced simultaneously. In the field, however, rainfall usually hinders the development of waves. In order to explain this contradiction of rainfall effect on waves, a possibility about energy transfer from turbulence to waves in case of the spectral peak of waves overlapping the inertial subrange of turbulence is assumed. It can be applied to interpret the damping phenomenon of gas transfer velocity in the laboratory experiments, and the variation of the TKE dissipation rates near sea surface compared with the law of wall.
Key words: rainfall, wind wave, wave age, turbulence, turbulent kinetic energy

Citation: Zhao Dongliang, Ma Xin, Liu Bin, Xie Lian. 2013. Rainfall effect on wind waves and a turbulence near an air-sea interface. Acta Oceanologica Sinica, 32(11): 10-20, doi: 10.1007/s13131-013-0372-7

1 Introduction

The rainfall on the ocean surface can change the air-sea interaction processes in several ways. Raindrops may produce both vertical and horizontal stresses on the water surface when they strike the moving water surface. The vertical stress is induced by the vertical impact velocity of raindrop. In the case of wind, the wind accelerates the raindrops in the horizontal direction, and produces the horizontal stress acting on the sea surface. The precise mechanisms of the phenomena are uncertain, but an enhancement of turbulence beneath the sea surface and the damping of surface gravity waves have been observed in laboratory experiments (Thorpe, 1995).

Reynolds (1900) suggested that the rain falling onto the sea surface tends to attenuate any surface gravity waves by mechanically mixing the upper layers of the water. Several studies argued that the horizontal stress induced by rain that might play as the role of wind stress may contribute to the generation of wind waves (Caldwell and Elliott, 1971; Le Méhauté and Khangaonkar, 1990). Many laboratory experiments have been conducted to investigate rain effects on surface waves, which generally confirmed the assertion of Reynolds (1900). Based on rain-mechanical wave systems, it was suggested that the waves are viscously damped by the turbulence generated by rain, in which the short waves are most severely attenuated by rain (Caldwell and Elliott, 1972; Houk and Green, 1976; Tsimplis and Thorpe, 1989; Tsimplis, 1992). By using an oval-shaped wind-wave tank, Poon et al. (1992) and Yang et al. (1997) found that the wind waves are damped by rain as a whole, but they are attenuated in gravity frequency range and enhanced at capillary frequency range. The whole damping effect decreases with the increase of wind speed. Ho et al. (2007) conducted their measurements in a standard wind-wave tank, and showed that the wind waves are attenuated over the full frequency range at low wind speed, and this damping effect is essentially not visible at their highest wind speed. To our knowledge, the variation of rain-induced turbulence in terms of the turbulent kinetic energy (TKE) dissipation rate has not been reported so far.

On the other hand, rainfall is expected to promote the gas transfer across the air-sea interface since it enhances turbulent mixing near the air-sea interface on the liquid side. Many studies showed that the gas transfer velocity correlates with the vertical stress by rain (Takagaki and Komori, 2007) or its equivalent quantity, the mean kinetic energy flux of raindrops impinging on the unit area of the air-sea interface (Ho et al., 1997; Ho et al., 2000). Recently, Zappa et al. (2009) suggested that TKE dissipation rate may be the most robust parameter to describe the gas transfer across the air-sea interface in various environmental conditions.

The present study tries to clarify the rain effect on the wind waves and the turbulence beneath the air-sea interface, especially at high wind speeds. It is first demonstrated the dual effect of rain on the generation and attenuation of wind waves occurring at different wind speeds. In order to explain the contradiction of rain effect on waves between laboratory and field

Foundation item: The National Basic Research Program of China under contract Nos 2009CB421201 and 2005CB422301; the National Natural Science Foundation of China under contract Nos 41076007, 40676014, 40490263 and 40830959.
*Corresponding author, E-mail: dlzhao@ouc.edu.cn

experiments, a possibility about energy transfer from turbulence to waves is proposed. The damping phenomenon of the gas transfer velocity reported by Komori et al. (1999), and the variations of the TKE dissipation rate beneath the sea surface compared with the law of wall are qualitatively interpreted by this possibility.

2 Experiments

2.1 *Experimental setup*

2.1.1 *Wind-wave tank*

The experiments were conducted in a large wind-wave tank (Fig. 1), which is situated in the Physical Oceanography Laboratory, Ocean University of China, Qingdao, China. The tank is 1.2 m wide, 1.5 m high and 65 m long, with a 48 m long working section. The water depth is 0.74 m during the experiments; tap water is used for all experiments. The tank is equipped with a programmable plunging-wedge wave maker, which allows for the computer-controlled generation of the mechanical wave packets. An artificial beach is placed at the end of the tank to dissipate wave energy in order to eliminate wave reflections. The wind tunnel is capable of up to 18 m/s wind speed in the centerline of the air space at the normal operating water depth.

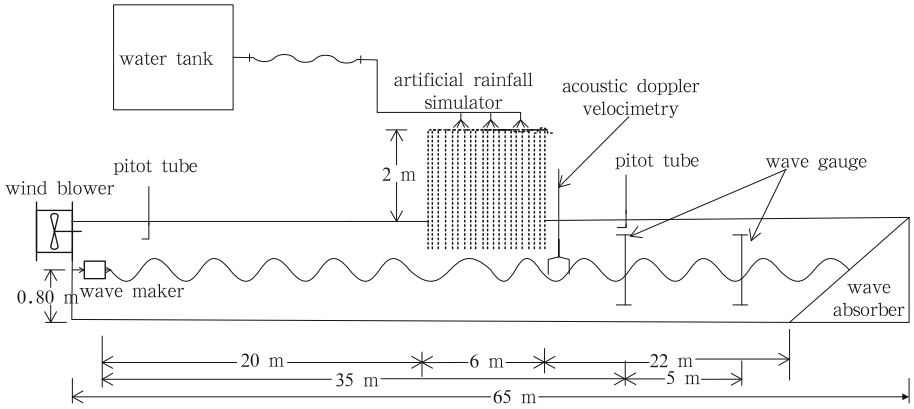

Fig.1. Schematic diagram of the laboratory setup.

2.1.2 *Artificial rainfall simulator*

The natural raindrops vary from the minute droplets in mist up to a maximum of 6 or 7 mm diameter, which is a physical upper limit of drop size and any drops with sizes above this limit are unstable and will break up into smaller drops. The median drop diameter by volume lies between 2 and 3 mm, and varies with intensity. Falling raindrops reach a maximum (or terminal) velocity when the force of gravitational acceleration equals the resistance of the drop falling through the air. The terminal velocity is a function of drop size and increases with the increase of drop size up to about 9 m/s for the largest drops.

Although ideally all physical characteristics of the natural rain are reproduced accurately in the laboratory, but there are always differences between the natural rain and the artificially produced rain in the laboratory. It is an accepted practice to use rain simulators with simplicity and low cost. Many rain simulators have used the principle of drops forming and dropping from the tip of tubes connected to a water supply (Takagaki and Komori, 2007). The advantage of this method is that the size of the drops and their fall velocity are constant, the distribution of rainfall across the test area is uniform and can be achieved with low water pressures. The disadvantage is that unless the device is raised up very high, the drops strike the test area at a velocity much lower than the terminal velocity of the natural falling rain. Another type of rain simulator is a spray from a watering tank. With pressure spray, the water leaves the nozzle with a velocity dependent on the pressure and then accelerates as it falls. The advantage of this type of spray is suitable for the stimulation of heavy rains as in the case of this study. Therefore, the second type of rain simulator was adopted in our experiments.

In our experiments, a water tank was used to supply water to the rainfall stimulator via a water pump. There was an electric adjustor controlling the flow rate to the nozzles. The system used for generating rain consisted of three pipes hanging off across the rainfall area. Attached to each pipe were six spray nozzles, for a total of 18 spray nozzles, which was switched on and off by three electromagnetic valves, for a total of nine electromagnetic valves. The diameters of nozzles on each pipe were the same, being 1, 2 and 3 mm, respectively, which represent the small and median raindrop sizes. The whole rainfall-area length was 6 m long, which was evenly divided into three segments. Each segment is 2 m long, and has six nozzles, which were independently controlled by three electromagnetic valves. In this way, the rainfall area can be adjusted for 2, 4 and 6 m long, respectively. The rainfall area was from 20 to 26 m down wind of the tank.

2.2 *Experimental conditions*

The experiments were conducted at wind speeds of U_r=5.33, 8.00 and 10.43 m/s, respectively, which were measured at 42 cm above the water surface. These wind speeds can be converted to U_{10}, i.e., the wind speed at 10 m by assuming a log profile. If it is assumed the drag coefficient $C_d = u^{*2}/U_{10}^2 = 1.2\times10^{-3}$, where u^* is the friction velocity of air, the three corresponding U_{10}=7.2, 10.9 and 14.2 m/s, which are the moderate to high wind speed commonly encountered at high latitudes. The measurements were performed at rain rates of 125, 260 and 310 mm/h as well as the case of absence of rain. For each rain rate, the rainfall-area lengths were changed by 2, 4 and 6 m, respectively. The wind was turned on for 20 min before any measurements were taken to ensure that a steady wind wave field was obtained. The waves, turbulence for both rain and no rain con-

ditions were measured at the same location downwind of the rainfall simulator. Hence the measured rain effects were solely due to the presence of rain.

2.3 *Measurements*

2.3.1 *Waves*

Waves at the tank were measured with two capacitance gauges (Fig. 1) and the signal was sampled at 25 Hz. The wave data presented here were taken from the wave gauge located 35 m down wind of the tank. With the fast Fourier transformation (FFT), the frequency spectra were calculated for 8 min records using Hanning windows of 8 s (200 points).

2.3.2 *Turbulence*

An acoustic Doppler velocimetry (ADV) was placed at 26 m down wind of the tank, immediately after the rainfall area, which was located at 10 cm under the water surface. The ADV measured three velocity components (u, v, and w, respectively) at 200 Hz. Turbulent velocity spectra were estimated by FFT from 12 min records.

In the steady flow with isotropic, fully developed turbulence, the kinetic energy is transferred from the mean flow to large eddies, then on to smaller eddies, and is finally dissipated by viscosity. Under these conditions, a common method for estimating the TKE dissipation rate ε in a turbulent flow is based on the existence of an inertial subrange that has a –5/3 slope, i.e.,

$$E(k) = \alpha\varepsilon^{2/3}k^{-5/3}, \tag{1}$$

where $E(k)$ is the one-dimensional wavenumber spectrum of the turbulent velocity, $k(=2\pi f/U_\mathrm{d})$ is the wavenumber in the mean flow U_d via the well-known Taylor's frozen turbulence hypothesis, f is frequency, and α is a Kolmogorov constant. Sreenivasan (1995) reviewed a large quantity of experimental data and found α=0.53 for longitudinal spectra, that is, the velocity in the same direction as k. In practice, the frequency spectrum $S(f)$ of turbulent velocity is usually measured instead of wave number spectrum where $E(k)\mathrm{d}k = S(f)\mathrm{d}f$. Hence the TKE dissipation rate ε can be calculated by

$$\varepsilon = 2\pi\alpha^{-3/2}U_\mathrm{d}^{-1}[S(f)f^{5/3}]^{3/2}. \tag{2}$$

Taylor's hypothesis is only valid for periods when the turbulent intensity is small relative to the mean flow. A generalization of Taylor's hypothesis to unsteady advection was used following Terray et al. (1996). It was taken that U_d is $\sqrt{2}$ times the rms vertical wave velocity and α=0.53 in our calculation.

3 Results

3.1 *Wave spectra and significant wave height*

Figure. 2 shows the frequency spectra of the wind waves at 35 m downwind of the wind blower. The spectra are significantly reduced over the full frequency range at the high rain rate and the low wind speed (Fig. 2a), which is consistent with that of Ho et al. (2007). This damping effect is independent of the rainfall-area length, and decreases with the wind speed. At the high wind speed, the enhancement effect of the rain on the wind waves is observed (Fig. 2b), which is different from the previous studies. In order to better demonstrate the rain effect on wind waves, the damping coefficient $\Delta(f)$ at various frequencies is calculated due to the presence of rain. Followed the method of Poon et al. (1992), $\Delta(f)$ is defined as

$$P(f)^{1/2} = P_0(f)^{1/2}\mathrm{e}^{-\Delta(f)}, \tag{3}$$

where $P(f)$ and $P_0(f)$ are wave spectra measured at the downwind region with and without rain, respectively. The results are shown in Fig. 3. Despite the scatter of the data, it can be seen from Fig. 3a that for the wind speed of 5.33 m/s, the damping coefficients are basically positive, which indicates the damping effect on the wind waves. The maximum damping occurs at about 1.7 Hz, which is a little lower than the spectral peak. On the other hand, although it is not so confirmed, it still can be seen from Fig. 3b that for the wind speed of 10.43 m/s, the damping coefficients are basically negative, especially for high frequencies, which indicates the waves are enhanced by the rain. It has been shown that wind input to the wind waves becomes negligible for frequencies lower than the spectral peak (Plant, 1982), in which the wave energy at these lower frequencies is obtained from waves at high frequencies above the spectral peak due to the nonlinear wave-wave interactions. Therefore, it can be inferred that, at low wind speed of 5.33 m/s, the

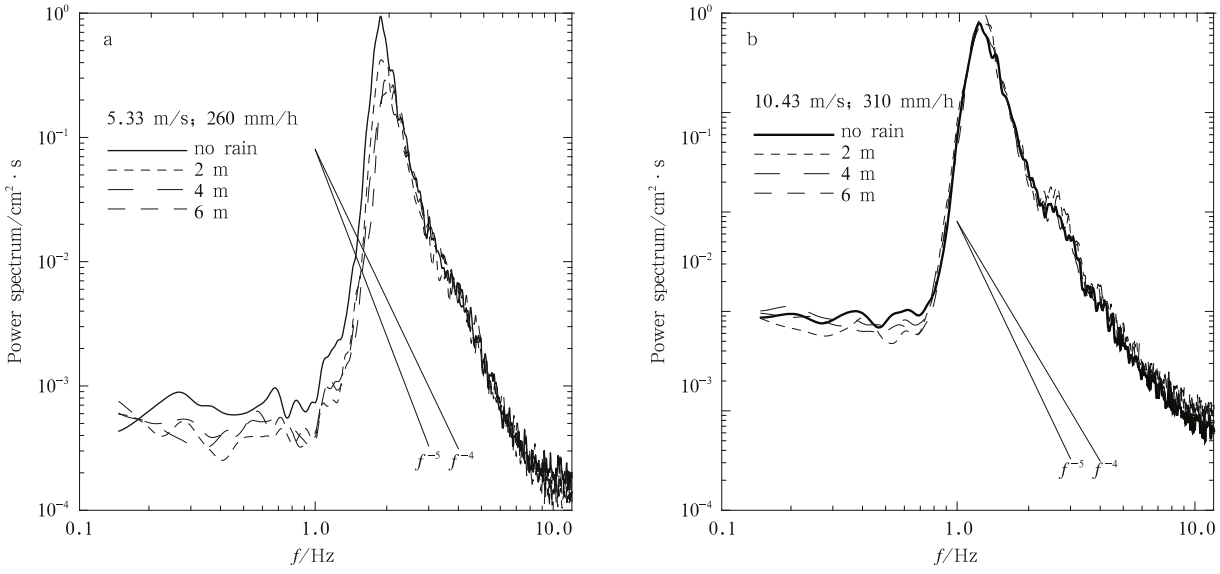

Fig.2. Wind wave spectra at wind speeds of 5.33 m/s with rain rate 260 mm/h (a), and 10.43 m/s with rain rate 310 mm/h (b).

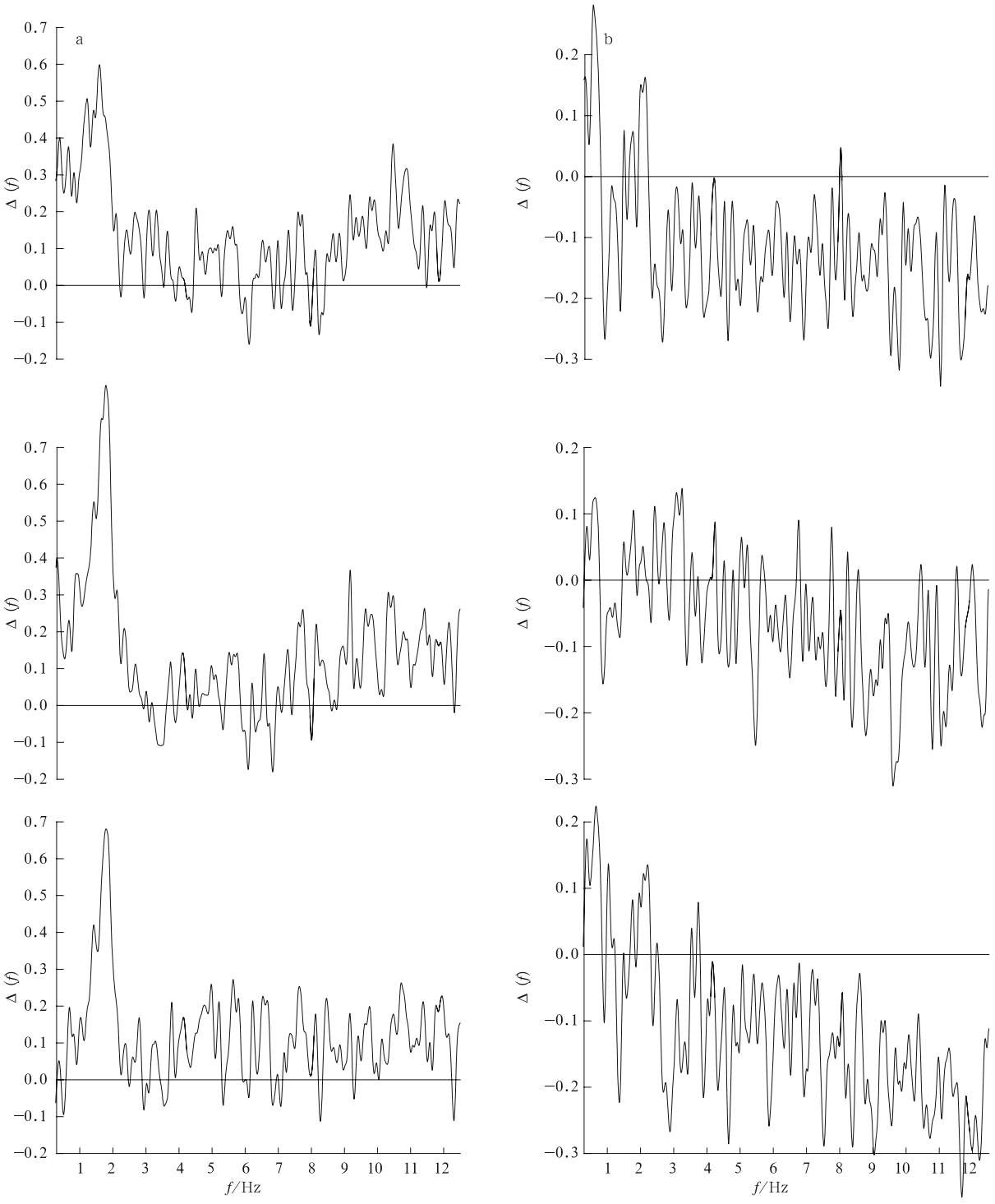

Fig.3. Damping coefficients at various frequencies. The wind speeds and rain rates are 5.33 m/s and 260 mm/h (a), and 10.43 m/s, 310 mm/h (b), respectively. The results from top to bottom are obtained at rainfall area lengths of 2, 4 and 6 m, respectively.

direct damping effect mainly occurs waves at high frequencies, which induces to weaken the nonlinear wave-wave interactions, and reduces the energy transfers to lower frequency waves from high frequency waves. Thus the damping of the lower frequency waves is an indirect effect of rainfall.

Here our discussion will be limited in the gravity waves with frequencies less than 6 Hz. Tsimplis (1992) found that the damping effects of rain on waves increase with the wave frequency in the absence of wind. With the lower wind speeds (less than 7 m/s) in a circulating wind-wave tank, Poon et al. (1992) and Yang et al. (1997) suggested the rain has damping effects on the gravity wind waves, which are reduced with the increase of wind speed in their experiment. In the present study, with a much higher wind speed of 10.43 m/s, the enhancement of

wind waves is observed.

In order to further identify the rain effect on the wind waves, the significant wave height H_s was calculated by the integral of the wave spectrum $P(f)$ through $H_s = 4\sqrt{\int P(f)\mathrm{d}f}$ with the integral limit up to 6 Hz. The comparison of H_s in the cases of different rain rates and no rain is shown in Fig. 4. It can be seen that the damping effect decreases with the wind speed. At the high wind speed, H_s is enhanced, instead of being damped by the rainfall. Both the damping and enhancement effects are obscured with rain rate, and are almost independent of the rainfall-area length.

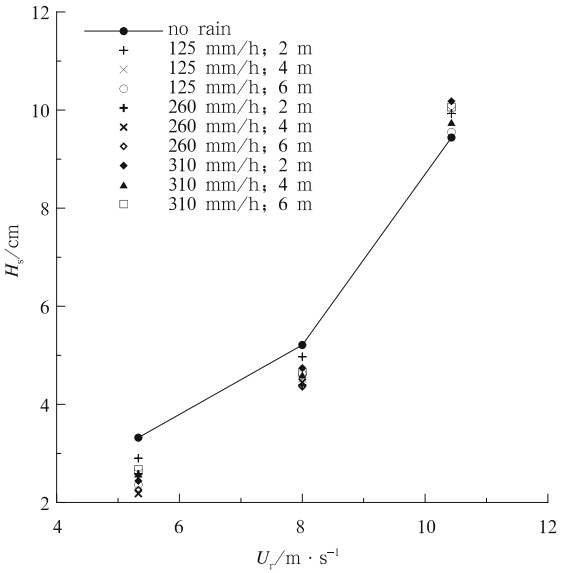

Fig.4. Comparison of significant wave height H_s with the cases of different rain rates and rainfall area lengths.

3.2 *Mean square slope of water surface*

The mean square slope (MSS) s^2 of the water surface is a description of the surface roughness that represents the interaction between the wind and wind waves. MSS can be directly calculated by the spectral moment of wave spectra (Phillips, 1977),

$$S^2 = \frac{(2\pi)^4}{g^2} m_4, \tag{4}$$

where $m_4 = \int f^4 P(f)\mathrm{d}f$ is the 4th spectral moment of frequency spectrum of the wind waves; and g is the gravity acceleration. The comparison of the MSS in the cases of rain and no rain is presented in Fig. 5. It is shown that the MSS increases drastically with increasing wind speeds for both rain and no-rain conditions. The damping effects on the MSS are most obvious at low wind speed, and decrease with the increase of wind speed. The decrease of MSS with the rain rate is obvious at the low wind speed. At the high wind speed, the enhancement of the MSS is observed instead of attenuation. The magnitude of the MSS via form drag over the waves supporting the surface stress represents the efficiency of the transfer of momentum flux from the air to the water. The higher the MSS, the more wind stress that can be used to generate wind waves. Therefore, the wave height generally increases with increasing MSS, and vice versa. The behavior of MSS confirms the attenuation and augment of wave height at different wind speeds as indicated in the preceding section.

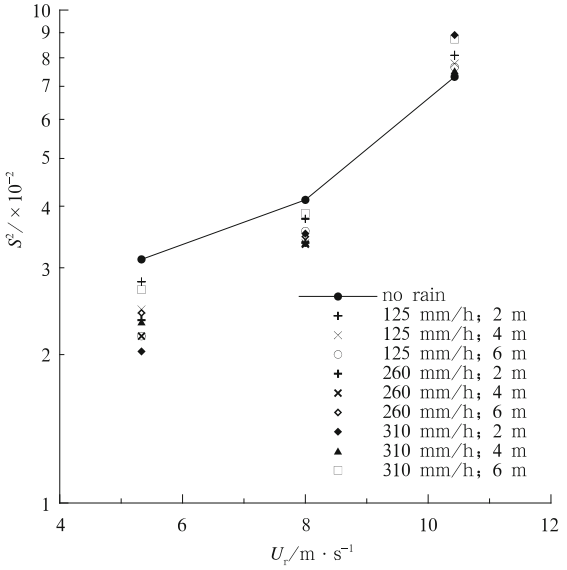

Fig.5. Comparison of mean square slope of water surface with and without rainfall.

3.3 *Turbulent velocity spectra and TKE dissipation rate*

The turbulent velocity spectra at wind speeds of 5.33 m/s and 10.43 m/s are shown in Fig. 6a, and b, respectively. It is noted that the turbulence is enhanced more significantly at the low wind speed (Fig. 6a) than the high wind speed (Fig. 6b), which is almost independent of the rainfall-area length. It can be seen that the turbulent energy is dominant in the frequency range of 0.01–0.1 Hz, which is much lower than the energy-containing wave frequency range (1–3 Hz). The turbulent velocity spectra have –5/3 slopes in the frequency rang of 0.1–1.0 Hz, which are considered to be the inertial subrange of the local isotropic turbulence (IST). These results are consistent with the previous laboratory studies (Yoshikawa et al., 1988; Mitsuyasu and Kusaba, 1985). There is an obvious spectral peak at about 2 Hz, which is believed to be associated with the spectral peak of the wind waves (SPW) through the orbital velocity. The turbulent energy is mainly contained in the frequency range lower than the SPW. In laboratory, the IST located at the lower frequencies than the SPW seems to be common for the very young wind waves from wind-wave tanks (Yoshikawa et al., 1988) or coastal ocean (Tokoro et al., 2008).

It is well known that the frequency at which IST behavior is observed increase with the mean flow speed and decrease with the scale of the dominant eddies. The latter is typically related to the distance from the interface, so the turbulent velocity spectra can be characterized by the parameter of fz/U_d, where z is the height from the surface. Trowbridge et al. (1999) showed that the IST begins at $fz/U_d > 10/2\pi$ or approximately 1, which can be used to confirm the existence of IST. As an example, Fig. 6a is plotted again versus the dimensionless frequency fz/U_d, and shown in Fig. 7, where z (=10 cm) is used. It can be seen that the IST behavior is still demonstrated. The frequencies at

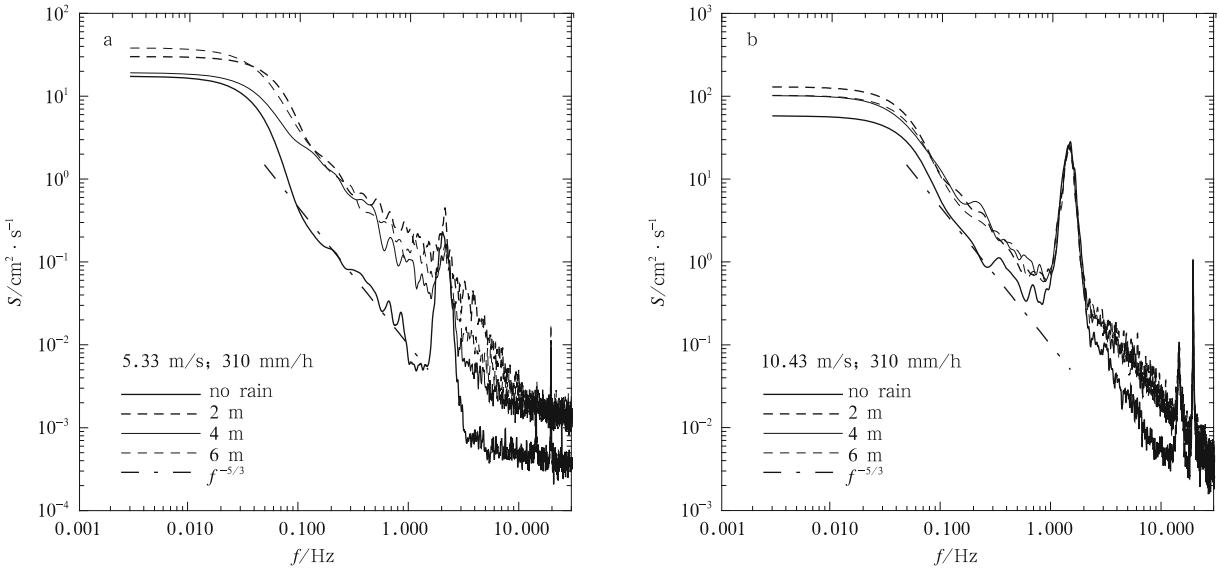

Fig.6. Turbulent velocity spectra at wind speeds of 5.33 m/s (a), and 10.43 m/s (b) with rain rate of 310 mm/h.

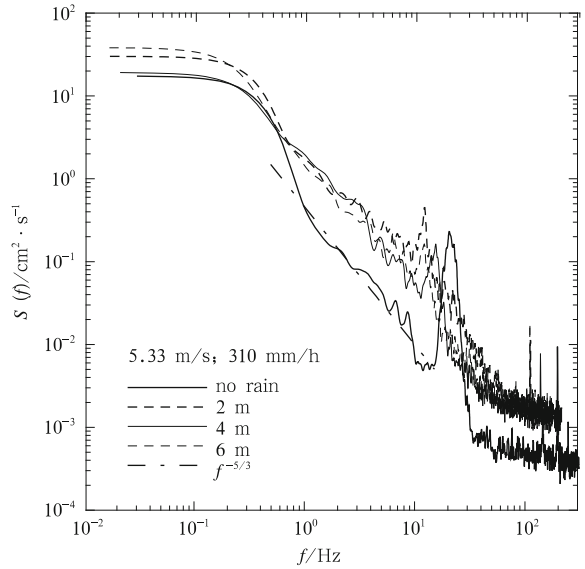

Fig.7. Turbulent velocity spectra versus fz/U_d. Here fz/U_d=1 when f=0.1 Hz, and fz/U_d=$10/2\pi$ when f=0.16 Hz.

which fz/U_d=$10/2\pi$ and 1 are 0.16 and 0.1 Hz, respectively. Therefore, the IST identified in Fig.6 is true, and can be used to calculate the TKE dissipation rate.

Figures 8a, b and c show the TKE dissipation rate with respect to the wind speed U_r, the rain rate R and the product of R and the rainfall-area length L, respectively. It can be seen that ε significantly increases with increasing wind speed, and enhances greatly with the rain rate at the low wind speed. However, ε increases slightly with the rain rate at the high wind speed (Fig. 8a). In general, ε is mainly determined by the wind speed, and also increases with the rain rate (Fig. 8b). Figure 8c shows that ε is almost independent of RL, which indicates that the variation of the rainfall-area length has little effect on the turbulent dissipation in the turbulence-wave interaction process.

4 Discussion

4.1 *Dual rain effect at different wind speeds*

As mentioned above, the dual effect of attenuation and generation of the wind waves at different wind speeds is identified in laboratory experiments. At the low wind speed, the wind waves as a whole are severely damped by the rain. With the increase of wind speed, the damping effect of rain decreases gradually. When the wind speed is sufficiently high, the wind waves, at least as a whole, are augmented, instead of damped, by the

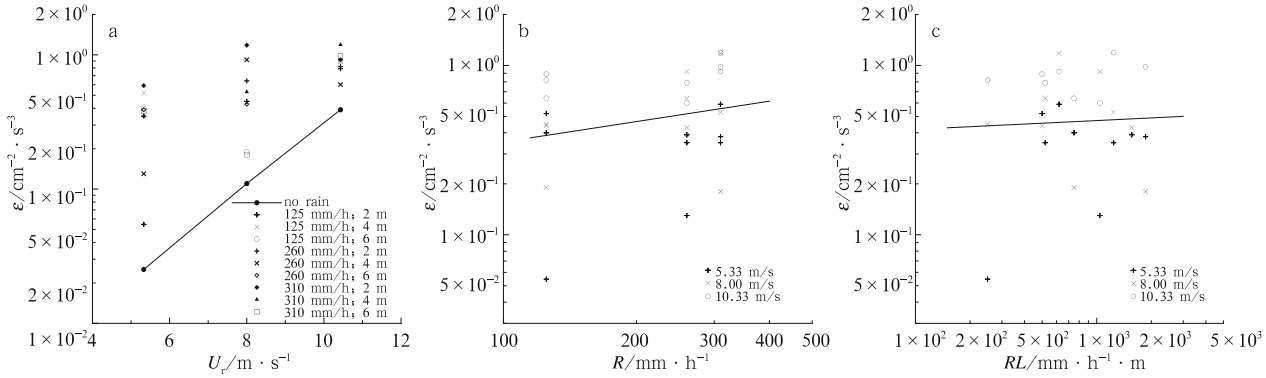

Fig.8. TKE dissipation rate ε versus wind speed U_r (a) rain rate R (b) and the product of rain rate R and rainfall area length L (c).

rain.

There are at least two ways that the rain can affect the motion in the water. First, the momentum flux of each raindrop gives rise to an average vertical stress within the water. Second, if there is a mean wind in the air, the horizontal momentum of each drop produces an average horizontal mass flux in the water in the direction of the wind. Caldwell and Elliott (1971) suggested that the horizontal impact velocity of raindrop is approximately 85% of the 10 m wind speed U_{10}, thus the horizontal stress carried by the rainfall can be written as

$$\tau_R = 0.85\rho_d R U_{10}, \tag{5}$$

where ρ_d is the density of raindrops. The vertical stress of the rain can be defined by (Yang et al., 1997; Takagaki and Komori, 2007)

$$MF = \rho_d R W_p, \tag{6}$$

where W_p is the vertical impact velocity of raindrops on the sea surface, which can be taken as the terminal velocity of rain drops in the field.

It is usually regarded that the vertical stress produces the pressure on the advancing waves and enhances turbulent dissipation of wind waves through the raindrops penetrating the free surface (Manton, 1973; Tsimplis and Thorpe, 1989; Tsimplis, 1992; Poon et al., 1992). On the other hand, Yang et al. (1997) suggested that the horizontal stress generates mean currents and enhances the gravity wind waves. Le Méhauté and Khangaonkar (1990) theoretically showed that the rain-induced horizontal stress can enhance the growth of high frequency waves, which is more significant at higher wind speeds.

Therefore, Yang et al. (1997) assumed that the horizontal and vertical stresses induced by rain compete with each other in the development of wind waves. At the lower wind speed, the horizontal stress is generally less than the vertical stress since the former linearly depends on the wind speed, thus the damping effect may dominate the enhancement effect, which leads to the attenuation of wind waves. The damping of longer wind waves may be a result of the weakening of nonlinear wave-wave interaction. When the wind speed U_{10} is high enough, for example, higher than 10 m/s, the horizontal stress that increases with the wind speed may dominate the effect of the vertical stress, since the maximum terminal velocity of the raindrop is about 9 m/s. In this situation, the wind waves will be enhanced, instead of damped, by the rain. This characteristic is clearly demonstrated in our experiments (Fig. 3).

To our knowledge, this dual effect of rain on waves as mentioned above, however, has not been observed in the field so far. Instead, it is a common knowledge among seafarers that rain "knocks down the sea" or attenuates the waves (Tsimplis and Thorpe, 1989). Satellite altimeters provide simultaneous observations for the wind speed, the wave height and the indicator sign of rain for a long time and large area of ocean. These data were divided into two groups by the cases of rain and no rain. In this way, it is possible to examine the rain effect on the waves in the field. The detailed discussions for the case of field will be given in another paper. One example that was obtained from the cycle 110 data of altimeter Janson-1 is shown in Fig. 9. With the work frequency at Ku band, the microwave wavelength is about 2.1 cm, the altimeter can detect the waves less than 9 Hz. Comparing the wave heights of rain and no rain conditions at the same wind speed, it is clearly demonstrated that rain damps the wave development at any wind speed, in which the damping effect increases with the increase of wind speed. This behavior obviously contradicts with that of the laboratory measurements presented above.

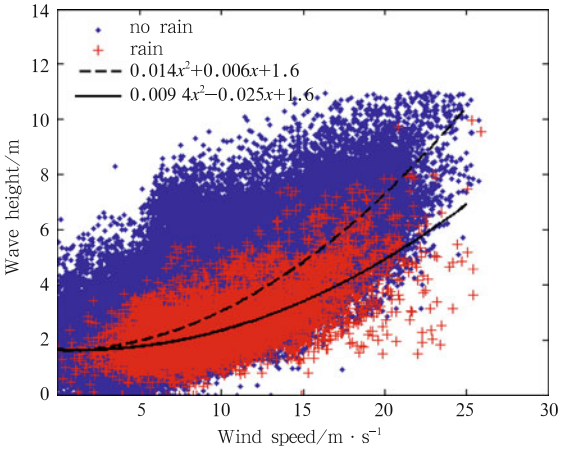

Fig.9. Damping effect of rain on the waves versus the wind speed in the field, which was derived from the observational data of altimeter Janson-1. The solid and dashed lines denote the best fit of the data in the case of rain and no rain, respectively.

On the other hand, the wind stress τ is quadratic with U_{10}, and can be written as

$$\tau = \rho_a C_d U_{10}^2, \tag{7}$$

where ρ_a is the density of air. Taken the typical values of ρ_a=1.2 kg/m^3, ρ_d=1 000 kg/m^3 and C_d=1.2×10^{-3}, the comparison of horizontal stress at rain rates of 25 and 50 mm/h and the wind stress is shown in Fig. 10. It is obvious that if the horizontal stress by rain actually plays the same role as the wind stress in the wave generation, the waves under the rain condition should be much greater than those at no rain conditions, especially at the low wind speed and the high rain rate, since the horizontal stress greatly exceeds the wind stress. Even in the case of the high wind speed (greater than 15 m/s), the horizontal stress still occupies a significant part of the wind stress that can not be ignored in observation and calculation. In practice, however, the significant generation of waves due to the heavy rain at the low wind speed has not been observed either in the field or in the laboratory. Instead, all of the laboratory experiments show that waves are damped at low wind speeds. Therefore, the rain-induced horizontal stress does not seem to significantly contribute to the generation of waves.

4.2 *Energy transfer from turbulence to waves*

All stresses, including the wind stress and the rain-induced stress, provide the energy to the water, thus the problem becomes how the energy input from the wind is distributed between the turbulence and the wave. Here the feedback effect of the sea surface on the wind is ignored for simplicity. The simultaneous wave damping and turbulence enhancement by the rain indicate that the energy input from the wind is transferred from wave to turbulence. On the contrary, when the waves are augmented and the turbulence enhancement is suppressed by rain at the same time, it is reasonable to regard that some energy is transferred from the turbulence to the waves in

order to explain this phenomena. If so, in what condition it will happen?

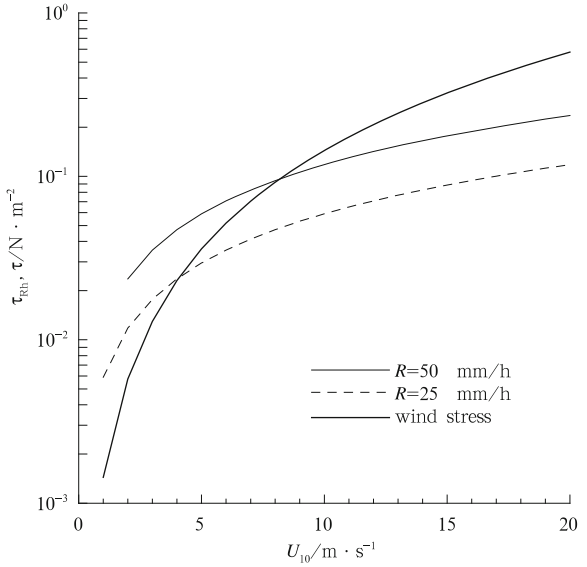

Fig.10. Comparison of the horizontal stress by the rain and the wind stress. The thin solid and dashed lines denote the horizontal stresses at rain rates of 50 and 25 mm/h, respectively.

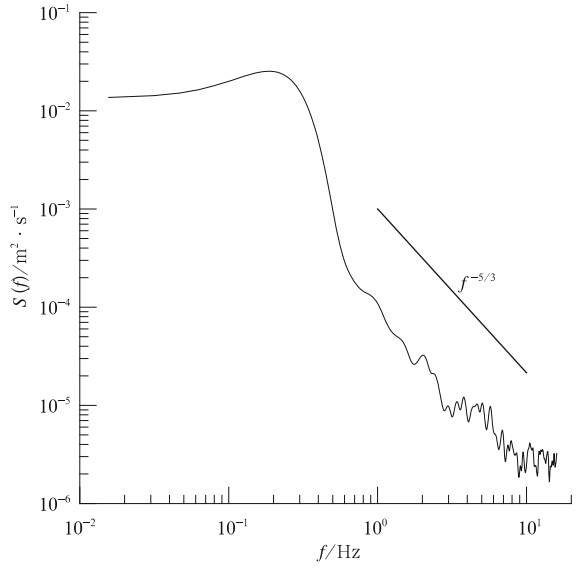

Fig.11. Turbulent velocity spectrum based on the data obtained at the Bohai Sea off the east coast of China.

Since the waves in the laboratory are usually much younger than those in the field, the SPW in the laboratory is generally higher in frequency than the SPW in the field. As a result, it is common that IST is located at the lower frequencies than the SPW in the case of laboratory (Yoshikawa et al., 1988). The present study (Fig. 6) and other laboratory studies (e.g., Mitsuyasu and Kusaba, 1985) further confirmed this assertion.

On the other hand, the IST is usually located at the higher frequencies than the SPW in the field (Agrawall et al., 1992; Terray et al., 1996; Drennan et al., 1996). This point was also identified by the ADV observational data obtained from Bohai Sea off the east coast of China. Figure 11 is an example of the turbulent velocity spectrum in Bohai Sea. It is shown that the IST is normally located in the frequency range of 1–10 Hz, which is in much higher frequency than the SPW in the field. Combined the situations in the laboratory and the field, the configuration of IST and SPW is schematically illustrated in Fig. 12.

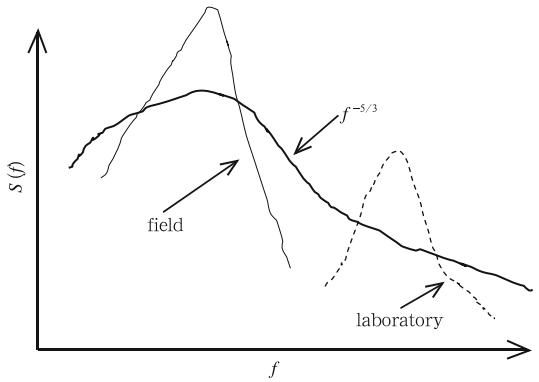

Fig.12. Schematic diagram of configuration of the SPW and the IST in the field and the laboratory.

It is well known that, with the increase of wind speed, the SPW gradually shifts to the lower frequency. Although the IST is also changed in frequency under different wind speeds, this variation should be less than the downshift of SPW. This leads to the big difference between the situations of laboratory and field. In the former, the decrease of SPW will approach or overlap the IST. In the latter, the decrease of SPW will separate further with the IST. The wave energy can transfer to the turbulence through the dissipation and the wave breaking. In contrast, it is usually regarded that the random turbulent energy cannot transfer to the ordered waves in general conditions. If it is assumed that there is a possibility that the turbulent energy can transfer to waves in the case of SPW overlapping IST, it is useful to explain the contradiction findings in laboratory and field discussed below.

In the laboratory, the IST and the SPW are separated away at low wind speed, thus the energy transfers from waves to turbulence as usual. As a result of keeping the energy balance in the system, the wave and the turbulence are simultaneously damped and enhanced, respectively. As the wind speed increases to certain level, the SPW moves to lower frequency, and is close to the IST. When they approach and overlap each other, some energy transfers from turbulence to waves, in which the waves are augmented and the enhancement of turbulence is reduced. Thus the waves in the laboratory are damped at the low wind speed, and enhanced at the high wind speed. In the field, however, since the IST is usually located at the higher frequency than the SPW, the downshift of the SPW makes it depart further from IST. As a result, the energy will usually transfer from the waves to the turbulence. Thus the waves in the field are generally attenuated by the rain due to the wave energy lost to the turbulence.

Therefore, it is suggested a mechanism that the energy transfers from the small scale motion to the large scale motion, which is reverse for the normal energy cascading process. Qiao and Zhang (1994) investigated the generation and development of the ocean shear wave in the area of the western boundary

current. They also found that the energy transfers from fluctuation motion to the mean motion due to the nonlinear interaction.

4.3 *TKE dissipation in the presence of waves*

A great deal of efforts has been directed toward determining the TKE dissipation rate in the upper oceanic layers since it is of great significance in matters of the mixing of near surface waters, gas transfer across the interface, dispersal of buoyant pollutants and the modeling of thermocline development. Before 1990, although a few reports show substantially higher levels of dissipation, the prevailing conceptual model of the ocean surface boundary layer regarded it as an inverted wall layer, in which the TKE dissipation rate follows

$$\varepsilon = u_{*\mathrm{w}}^3/\kappa z, \tag{8}$$

where $u_{*\mathrm{w}}$ is the friction velocity of water; κ the von Kármán constant, 0.4; and z the depth. Afterwards, more and more studies suggested that the enhanced dissipation due to wave and its breaking exceeds the wall layer values by one or two orders of magnitude in moderate and strong wind conditions (Anis and Moum, 1995; Terray et al., 1996), i.e., $\varepsilon/(u_{*\mathrm{w}}^3/\kappa z) \gg 1$. With a close inspection, however, it is also found that some of the TKE dissipation rates under waves are less than the wall layer values, i.e., $\varepsilon/(u_{*\mathrm{w}}^3/\kappa z) < 1$. These behaviors of the turbulence were clearly identified in Fig. 4 of Anis and Moum (1995) and Table 2 of Thorpe et al. (2003).

Based on the usual knowledge, it is difficult to explain the reduced turbulent energy because the turbulence should obtain extra energy from waves and the TKE dissipation rate under wind waves should be greater than or equal to the law of wall. Where the turbulent energy is gone? Here it is suggested that there is a possibility that the turbulent energy can transfer to waves in the case of SPW and IST overlapping. In the field, this situation can only happen when the wind waves are very young, and the SPW is high enough to approach IST. It needs to find evidence to show that $\varepsilon/(u_{*\mathrm{w}}^3/\kappa z) < 1$ for the wind waves at the small wave age.

However, it is difficult to find the very young wind waves in the field because of the long fetch usually encountered, which makes the field waves much developed with high wave ages. Based on the field measurements on a lake, Terray et al. (1996) proposed a scaling for the TKE dissipation rate near the sea surface:

$$\varepsilon = 0.3 u_{*\mathrm{w}}^2 \overline{c} H_\mathrm{s} (H_\mathrm{s}/z)^2, \tag{9}$$

where $\overline{c}$ is called the effective phase speed, which correlates with the phase speed of waves at the spectral peak. In order to compare with the law of wall, Eq. (9) can be rewritten as

$$\frac{\varepsilon}{u_{*\mathrm{w}}^3/\kappa z} = 0.14 \left(\frac{\overline{c}}{u_{*\mathrm{w}}}\right)\left(\frac{H_\mathrm{s}}{z}\right). \tag{10}$$

The first parenthesis on the right side of Eq. (10) represents a kind of wave age. The younger the wave, the smaller the wave age is. The young wave generally corresponds to small H_s. It is clear that the greatest possibility of $\varepsilon/(u_{*\mathrm{w}}^3/\kappa z) < 1$ is in the case of young waves. On the contrary, the mature waves have large wave age and H_s, which makes $\varepsilon/(u_{*\mathrm{w}}^3/\kappa z)$ potentially greater than 1.

The quantitative evidence is given by Thorpe et al. (2003). They investigated the TKE dissipation rate limited by fetch to 26 km, in which the young waves were observed. Based on the data in their Table 2, the TKE dissipation rates versus the wave age are plotted in Fig. 13. It is shown that $\varepsilon/(u_{*\mathrm{w}}^3/\kappa z) < 1$ when the wave age c/u_* is smaller than about 17.

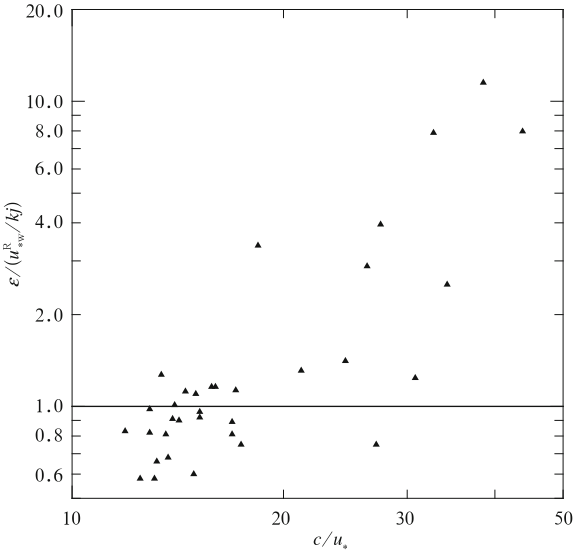

Fig.13. The variation of $\varepsilon/(u_{*\mathrm{w}}^3/\kappa z)$ with the wave age c/u_* based on the observational data of Thorpe et al.(2003).

4.4 *Implications to gas transfer*

It is believed that the turbulent intensity near the sea surface directly controls the gas transfer through the air-sea interface. By using the thickness of the viscous and diffusive sublayers in terms of the Kolmogorov and Batchelor length scales, Lorke and Peeters (2006) suggested that the interfacial fluxes at both the benthic and air-sea boundary layers can be described by a unified relationship, in which the gas transfer velocity k_L can be expressed as

$$k_\mathrm{L} = (2\pi)^{-1} Sc^{-1/2} (\varepsilon \nu)^{1/4}, \tag{11}$$

where the Schmidt number Sc is defined as the ratio of the kinematic viscosity ν of water to the mass diffusivity D. A similar scaling has been derived by Kitaigorodskii (1984) in the context of modeling the influence of patches of the enhanced turbulence by the wave breaking, and by Lamont and Scott (1970) using surface renewal theory.

Therefore, all factors, such as wind speed, wave and current, which can influence the turbulence, are expected to correlate with the gas transfer velocity. The TKE dissipation rate is regarded as the most robust parameter to all the modifications and transforms to the turbulence (Zappa et al., 2009). However, the gas transfer velocity has been traditionally expressed as a function of the wind speed for practical applications since the wind is the main factor driving the turbulence, as well as easily obtained from routine observations. With a series of laboratory experiments in a wind-wave tank, Komori et al. (1999) measured the gas transfer velocity in the wind speed U_r range of 2 to 20 m/s. They found that the gas transfer velocity rapidly increases with the increase of wind speed when U_r <5 m/s. However, the gas transfer velocity tends to be damped in the wind speed range of 5 m/s< U_r <12 m/s. For the higher wind

speeds of U_r >12 m/s, gas transfer velocity again begins to increase rapidly (see their Fig. 3).

This damping phenomenon of the gas transfer velocity in terms of the wind speed can also be interpreted by the possibility of energy transfer from turbulence to waves mentioned above. At the low wind speed, the SPW is located at higher frequency than that of the IST, and separated from the IST. The energy transfers from wave to turbulence as usual. The significant enhancement of turbulence leads to the rapid increase of the gas transfer velocity with the wind speed. When the wind speed is high enough, the SPW moves to lower frequency until it approaches and overlaps with the IST. Then the energy starts to transfer from turbulence to wave. Thus the turbulence enhancement is greatly hindered; the corresponding gas transfer velocity tends to level off in this wind speed range. When the wind speed becomes much higher, the SPW departs from the IST by moving to much lower frequency, the energy again transfers from wave to turbulence, which leads to rapidly increasing the TKE dissipation rate. Thus the gas transfer velocity rapidly increases with the wind speed again.

Therefore, it is inferred that the damping phenomenon of the gas transfer velocity discovered by Komori et al. (1999) is a result of the parameterization of the gas transfer velocity in terms of the wind speed. It is the turbulent intensity or the TKE dissipation rate, not wind speed, which directly controls the gas transfer through the air-sea interface. If the gas transfer velocity was parameterized in terms of the TKE dissipation rate, this damping phenomenon would disappear.

5 Conclusions

The rain effects on the wind waves and the turbulence beneath the sea surface were investigated by laboratory experiments in various wind speeds, rain rates and rainfall-area lengths. It is shown that the rain effects on the waves depend on the wind speeds and the rain rates, but are almost independent of the rainfall-area lengths. The surface roughness in terms of the mean square slope of sea surface is well correlated with the wave development at all wind speeds. In laboratory, the wind waves are damped as a whole at the low wind speeds, but are enhanced at the high wind speeds. Simultaneously, the TKE dissipation rates are significantly increased with the rain rates at the low wind speeds, and their arguments are not obvious at the high wind speeds. The dual effect of rain on the waves has not been found in the field so far. Instead, the field waves are generally attenuated at low and high wind speeds. This damping effect is more significant with the increase of wind speed.

In order to explain this contradiction, a possibility of energy transfer from turbulence to waves is assumed in the case of the SPW overlapping the IST, although it remains to confirm in the future. It is useful to interpret the damping phenomenon of the gas transfer velocity in terms of wind speed, and the damping TKE compared with the law of wall when the wind waves are very young.

The important contributions of this work are: (1) first demonstration that the wind waves are enhanced at the high wind speeds in laboratory, and the corresponding turbulence enhancement is suppressed, and (2) the proposal of a possibility of the energy transfer from turbulence to waves. It provides a new approach to clarify the turbulence-wave interaction process.

References

Agrawal Y, Terray E, Donelan M, et al. 1992. Enhanced dissipation of kinetic energy beneath surface waves. Nature, 359: 219–220

Anis A, Moum J N. 1995. Surface wave-turbulence interactions: scaling $\varepsilon(z)$ near the sea surface. Journal of Physical Oceanography, 25: 2025–2045

Caldwell D R, Elliott W P. 1971. Surface stresses produced by rainfall. Journal of Physical Oceanography, 1(2): 145–148

Caldwell D R, Elliott W P. 1972. The effect of rainfall on the wind in the surface layer. Boundary Layer Meteorology, 3: 146–151

Drennan W M, Donelan M A, Terray E A, et al. 1996. Oceanic turbulence dissipation measurements in SWADE. Journal of Physical Oceanography, 26: 808–815

Ho D T, Asher W E, Bliven L F, et al. 2000. On mechanisms of rain-induced air-water gas exchange. Journal of Geophysical Research, 105: 24045–24057

Ho D T, Bliven L F, Wanninkhof R, et al. 1997. The effect of rain on air-water gas exchange. Tellus, 49B: 149–158

Ho D T, Veron F, Harrison E, et al. 2007. The combined effect of rain and wind on air-water gas exchange: A feasibility study. Journal of Marine Systems, 66: 150–160

Houk D, Green T. 1976. A note on surface waves due to rain. Journal of Geophysical Research, 81(24): 4482–4484

Kitaigorodskii S A. 1984. On the fluid dynamical theory of turbulent gas transfer across an air-sea interface in the presence of breaking wind-waves. Journal of Physical Oceanography, 14(5): 960–972

Komori S, Shimada T, Misumi R. 1999. Turbulence structure and mass transfer at a wind-driven air-water interface. In: Sajjiadi S G, Thomas N H, Hunt J C R, eds. Wind over Wave Couplings: Perspectives and Prospects. Oxford: Clarendon Press, 273–285

Lamont J C, Scott D S. 1970. An eddy cell model of mass transfer into the surface of a turbulent liquid. AIChE Journal, 16: 512–519

Le Méhauté B L, Khangaonkar T. 1990. Dynamic interaction of intense rain with water waves. Journal of Physical Oceanography, 20: 1805–1812

Lorke A, Peeters F. 2006. Toward a unified scaling relation for interfacial fluxes. Journal of Physical Oceanography, 36: 955–961

Manton M J. 1973. On the attenuation of sea waves by rain. Geophysical Fluid Dynamics, 5: 249–260

Mitsuyasu H, Kusaba T. 1985. Wind waves and wind-generated turbulence in the water. In: Toba Y Mitsuyasu H, eds. The Ocean Surface. Dordrecht: D. Reidel Publish Company, 389–394

Phillips O M. 1977. The dynamics of the upper ocean. Cambridge: Cambridge University Press, 336

Plant W J. 1982. A relationship between wind stress and wave slope. Journal of Geophysical Research, 87: 1961–1967

Poon Y K, Tang S, Wu J. 1992. Interactions between rain and wind waves. Journal of Physical Oceanography, 22: 976–987

Qiao Fangli, Zhang Qinghua. 1994. A model for the generation and development of ocean shear wave. Acta Oceanologica Sinica (in Chinese), 16(5): 11–24

Reynolds O. 1900. Papers on Mechanics and Physical Subjects. Vol. I. Cambridge: Cambridge University Press, 86

Sreenivasan K R. 1995. On the universality of the Kolmogorov constant. Physical Fluids, 7: 2778–2784

Takagaki N, Komori S. 2007. Effects of rainfall on mass transfer across the air-water interface. Journal of Geophysical Research, 112: C06006, doi:10.1029/2006JC003752

Terray E A, Donelan M A, Agrawal Y C, et al. 1996. Estimates of kinetic energy dissipation under breaking waves. Journal of Physical Oceanography, 26: 792–807

Thorpe S A. 1995. Dynamical processes of transfer at the sea surface. Progress of Oceanography, 35: 315–352

Thorpe S A, Osborn T R, Jackson J F E, et al. 2003. Mesurements of turbulence in the upper-ocean mixing layer using Autosub. Journal of Physical Oceanography, 33: 122–145

Tokoro T, Kayanne H, Watanabe A, et al. 2008. High gas transfer velocity in coastal regions with high energy-dissipation rates. Journal of Geophysical Research, 113: C11006, doi: 10.1029/2007JC004528

Trowbridge J H, Geyer W R, Bowen M M, et al. 1999. Near-bottom turbulence measurements in a partially mixed estuary: turbulent energy balance, velocity structure, and along-channel momentum balance. Journal of Physical Oceanography, 29: 3056–3072

Tsimplis M N. 1992. The effect of rain in calming the sea. Journal of Physical Oceanography, 22: 404–412

Tsimplis M N, Thorpe S A. 1989. Wave damping by rain. Nature, 342: 893–895

Yang Z, Tang S, Wu J. 1997. An experimental study of rain effects on fine structures of wind waves. Journal of Physical Oceanography, 27: 419–430

Yoshikawa, I, Kawamura H, Okuda K, et al. 1988. Turbulent structure in water under laboratory wind waves. Journal of Oceanography Society of Japan, 44: 143–156

Zappa C J, Ho D T, McGillis W R, et al. 2009. Rain-induced turbulence and air-sea gas transfer. Journal of Geophysical Research, 114: C07009, doi: 10.1029/2008JC005008